Steady State Performance of a Large Capacity Pulse Motor Driven by Current Controlled PWM Inverter

Yoshitaka MINARI and Katsuji SHINOHARA

(Received May 30, 1996)

Abstract

A pulse motor is generally used for a small capacity drive system. The paper describes the proper motor structure and drive circuit for a large capacity pulse motor. The structure of armature winding is improved for the purpose of decreasing copper loss. The new drive circuit using a current controlled PWM inverter is proposed. There are four power transistors in the inverter, and four phase armature windings are connected in series with the power transistors respectively. The voltage and current waveforms and the steady atate characteristics of the pull-out torques etc. are obtained from analysis on the heteropolar type pulse motor. The advantages of this system are confirmed by the calculations and experimental results.

1. Introduction

The pulse motors are in use for the open-loop precise positioning cortrol since it is excellent in the start-stop performance and high reliability. Because of the small maintenance and low cost, the pulse motor is superior to DC motor used for the closed-loop positioning control, and it occupies an important demand in the digital computers etc. However, this trend is generally appropriate for the small capacity pulse motor. Previously one of the authors has proposed the large capacity pulse motor drive system [1, 2]. Then the armature winding was constructed with the conventional bifilar wound coil, and the four phase armature windings were connected to current source inverter with additional chopper circuit. In this paper, the number of coils of armature windings per pole in the proposed machines is reduced by half; therefore the copper loss decreased as shown in Appendices 8.1. The improvements of armature winding in the three DC excitation types are illustrated comparing with conventional form which has two armature coils per pole. The main circuit of new drive system which has four power transistors is simplified in order for an additional chopper circuit to disappear. A similar circuit has been used in variable reluctance motor [3].

Recently, the investigations in the pull-out torque performances etc. have been represented in consideration of the excitation mode and system parameters about the variable reluctance stepping motor [4-6]. As concerns hybrid stepping motor, the steady state analysis and the calculations and experiments of the pull-out torque have been performed [7-9].

This paper presents the steady state characteristics of the DC excitation type pulse motor driven by the new drive circuit. The circuit operations and steady state performances based on a machine parameter are presented first. Secondly, the calculated and experimental results of the induced voltage and winding current waveforms and the pull-out torque are shown.

2. Improvement of motor windings and inductance matrix

2.1 Improvement of motor windings

Figure 1 shows the comparison of conventional and new form concerning motor winding connections. This illustrates a variable reluctance type and three types of DC excitation, i.e. heteropolar, bipolar and homopolar type. In the new form of the DC excitation types, the number of armature coils decreases. Fig. 2 shows the contrast of conventional and new form about magnetomotive force distribution of air gap. In this case, $f_1/a_1=4$ and $f_2/a_2=1.5$ because of the equal mmf distributions in the two forms, where f_1 and f_2 are turn ratios of DC excitation winding turn to the total turns per pole, and a_1 and a_2 are turn ratios of armature winding turn to the total turns per pole. The total turn of conventional form considers one armature coil between the two. Suffix 1 denotes the conventional form and 2 the new. The following relations hold on condition that the magnetomotive force distribution in DC excitation type shown in conventional form is equivalent to one in new form.

$$a_2=2a_1$$

$$f_2=f_1-a_1 \tag{1}$$

The turn ratio of the new windings to the conventional windings is given by

$$\frac{a_2+f_2}{2a_1+f_1}=\frac{a_1+f_1}{2a_1+f_1} \tag{2}$$

for instance, this is 0.75 with $f_1/a_1=2$. Therefore, the sectional area of conductor wire will enlarge, and the copper loss becomes smaller (See Appendices 8.1). This makes the system advantageous with regard to temperature rise of motor.

2.2 Inductance matrix

Inductance matrix of the motors is obtained by similar method in reference [1] (See Appendices 8.2). These are shown in Table 1. Inductance matrix of variable reluctance type motor is represented by 4×4 matrix except the 5th row and column in the heteropolar type matrix, this is guessed from Fig. 1. In the Table, N is total turn per pole, λ_c is DC component of air-gap permeance per pole, λ_{max} is maximum value of air-gap permeance per pole and λ_{min} is minimum value of air-gap permeance per pole.

3. Drive circuit

3.1 circuit configuration

Drive circuit consists of power section and signal section as shown in Fig. 3. The power section is composed of rectifier circuit, smoothing circuit, PWM switching circuit, motor armature windings, feedback and freewheeling circuit, DC excitation windings (field windings), series reactor and current detecting resistor. Diode D1~D4 protect the inverse voltage to power transistor. The signal section is composed of pulse frequency divider, commutation pulse generator, constant current chopper, signal synthesizer and amplifier. The commutation pulse generator is specific work for pulse motor drive circuit. The commutation of armature current is severe because the commutation inductance is larger owing to motor structure; therefore it is necessary to apply as long as possible the

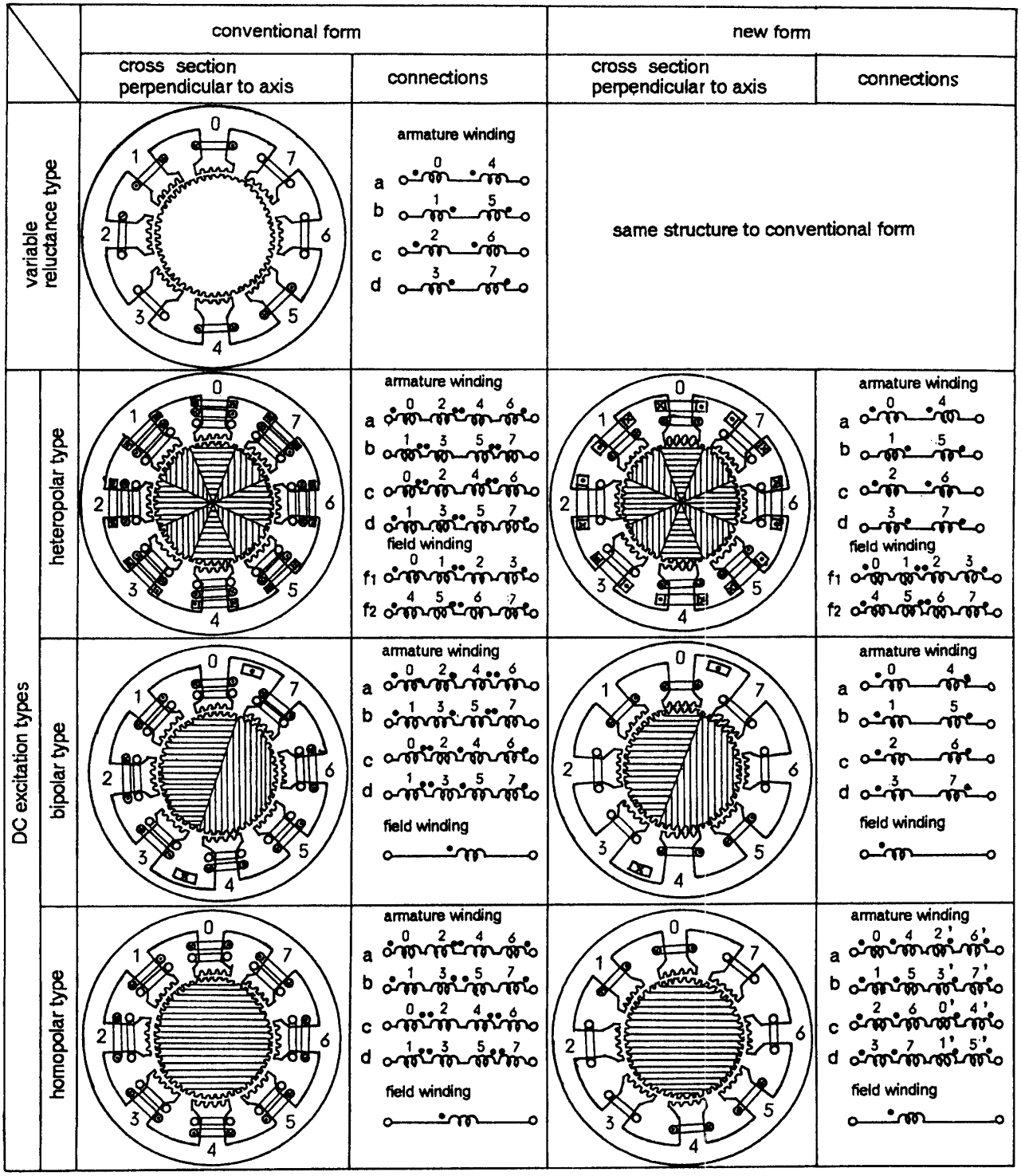

Armature coil 2', 6', etc. denote one of a pair halved on axial direction in the new homopolar type.

Each part of hatching shows the pole N or S due to field winding.

Fig. 1 Comparisons of motor coil connection

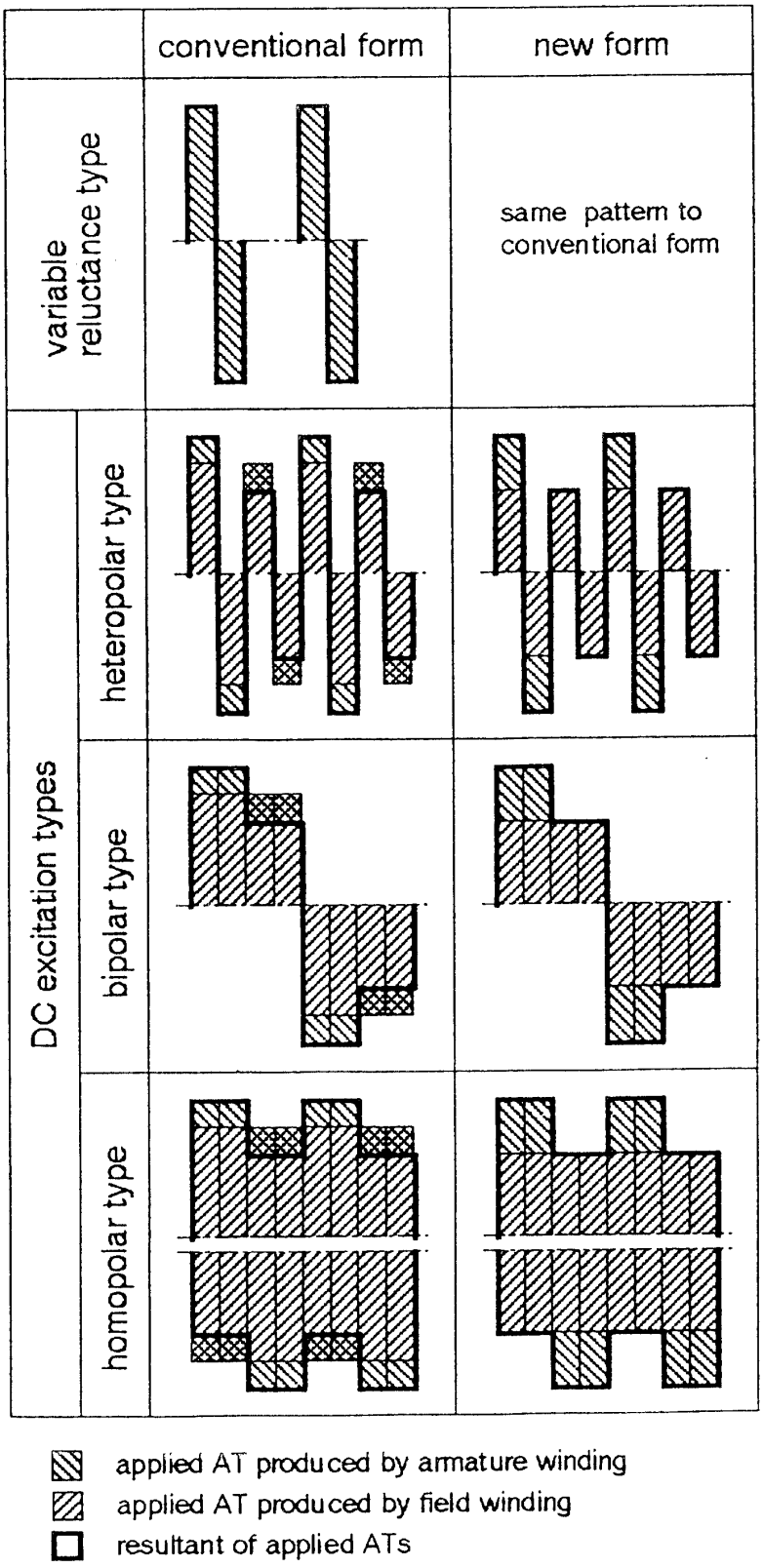

Fig. 2 Magnetomotive force of air gap

Table 1: Calculation of inductance matrices

DC excitation types	inductance matrix
heteropolar type	$a_2^2 L_c \left\{ \frac{1}{4} \begin{bmatrix} 3-\frac{K^2}{2} & 1 & -1+\frac{K^2}{2} & 1 & 4h \\ 1 & 3-\frac{K^2}{2} & 1 & -1+\frac{K^2}{2} & 4h \\ -1+\frac{K^2}{2} & 1 & 3-\frac{K^2}{2} & 1 & 4h \\ 1 & -1+\frac{K^2}{2} & 1 & 3-\frac{K^2}{2} & 4h \\ 4h & 4h & 4h & 4h & 16h^2 \end{bmatrix} + \frac{K}{4} \Re \left\{ \begin{bmatrix} 2\gamma^0 & \gamma^0+\gamma^3 & 0 & \gamma^0+\gamma^1 & 4\gamma^0 h \\ \gamma^3+\gamma^0 & 2\gamma^3 & \gamma^3+\gamma^2 & 0 & 4\gamma^3 h \\ 0 & \gamma^2+\gamma^3 & 2\gamma^2 & \gamma^2+\gamma^1 & 4\gamma^2 h \\ \gamma^1+\gamma^0 & 0 & \gamma^1+\gamma^2 & 2\gamma^1 & 4\gamma^1 h \\ 4\gamma^0 h & 4\gamma^3 h & 4\gamma^2 h & 4\gamma^1 h & 0 \end{bmatrix} e^{j\theta_e} \right\} - \frac{K^2}{8} \Re \left\{ \begin{bmatrix} \gamma^0 & -\gamma^3 & \gamma^2 & -\gamma^1 & 0 \\ -\gamma^3 & \gamma^2 & -\gamma^1 & \gamma^0 & 0 \\ \gamma^2 & -\gamma^1 & \gamma^0 & -\gamma^3 & 0 \\ -\gamma^1 & \gamma^0 & -\gamma^3 & \gamma^2 & 0 \\ 0 & 0 & 0 & 0 & 0 \end{bmatrix} e^{j2\theta_e} \right\} \right\}$
bipolar and homopolar types	$a_2^2 L_c \left\{ \begin{bmatrix} 1 & 0 & 0 & 0 & h \\ 0 & 1 & 0 & 0 & h \\ 0 & 0 & 1 & 0 & h \\ 0 & 0 & 0 & 1 & h \\ h & h & h & h & 4h^2 \end{bmatrix} + K \Re \left\{ \begin{bmatrix} \gamma^0 & 0 & 0 & 0 & \gamma^0 h \\ 0 & \gamma^3 & 0 & 0 & \gamma^3 h \\ 0 & 0 & \gamma^2 & 0 & \gamma^2 h \\ 0 & 0 & 0 & \gamma^1 & \gamma^1 h \\ \gamma^0 h & \gamma^3 h & \gamma^2 h & \gamma^1 h & 0 \end{bmatrix} e^{j\theta_e} \right\} \right\}$

notations :

$h = \frac{L_2}{a_2}$, $L_c = 2 N^2 \lambda_c$

$K = \frac{\lambda_{max} - \lambda_{min}}{\lambda_{max} + \lambda_{min}}$

$\gamma^m = \left(e^{j 2\pi/4} \right)^m$ $(m = 0, 1, 2, 3)$

$\Re$ = real part

θ_e = rotating angle of rotor in electrical angle

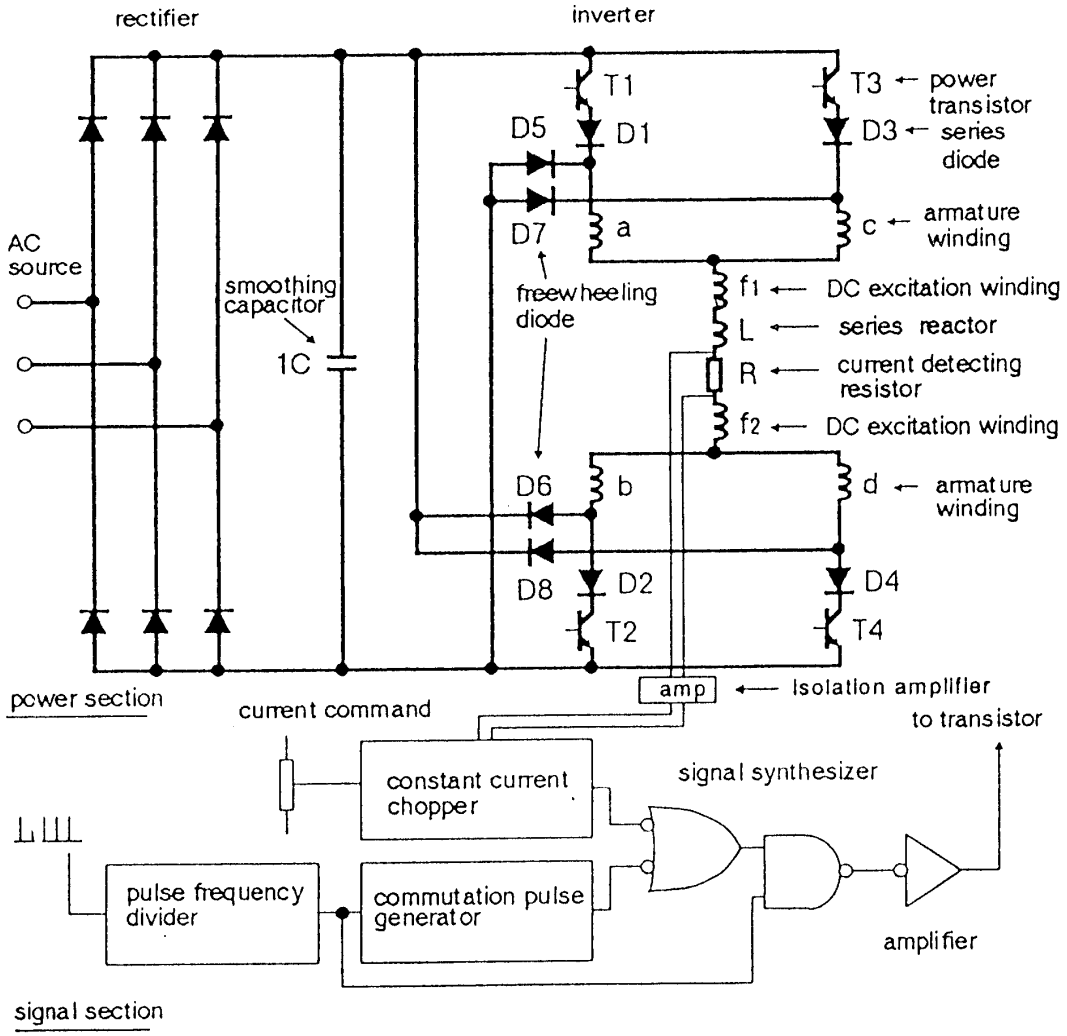

Fig. 3 Drive circuit

higher voltage to commutation winding in order to protect the motor torque reduction in the high speed region. The commutation voltage is determined by input source voltage, and maximum interval of applied commutation voltage is 90° in electrical angle shown in Fig. 4 (A) and Fig. 5 (A). If this interval comes to pass 90° in electrical angle, the upper and lower arm transistors of drive circuit are on-state at the same time. In this case, the power control with constant current of winding becomes impossible. The commutation pulse must be given in the first half period of the putput of pulse frequency divider so as to quicken the armature current commutation, so that the large output torque is obtained in the high speed region.

3.2 Circuit operations

Circuit operations are classified into two states from overlap angle u of commutation as the following explanations.

(1) $u \leq 90°$ (refer to Fig. 4 (A) and Fig. 4 (B))

~0: phase c is on-state of chopper signal, and the commutation pulse is applied to phase d, so that active power flows into the motor.

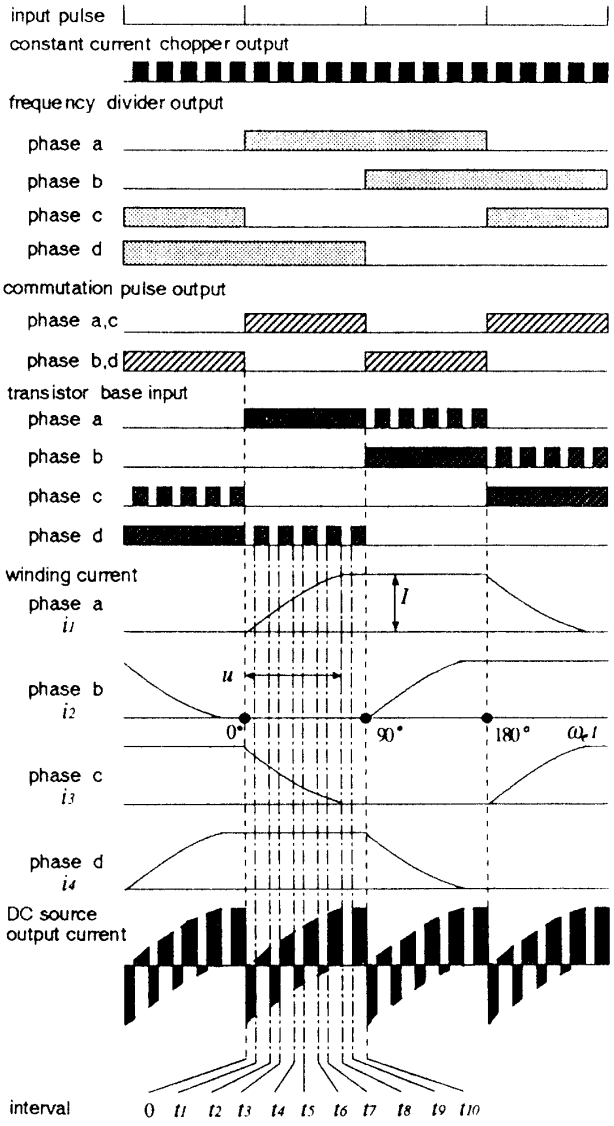

Fig. 4(A) Control signal and current waveforms ($u \leq 90°$)

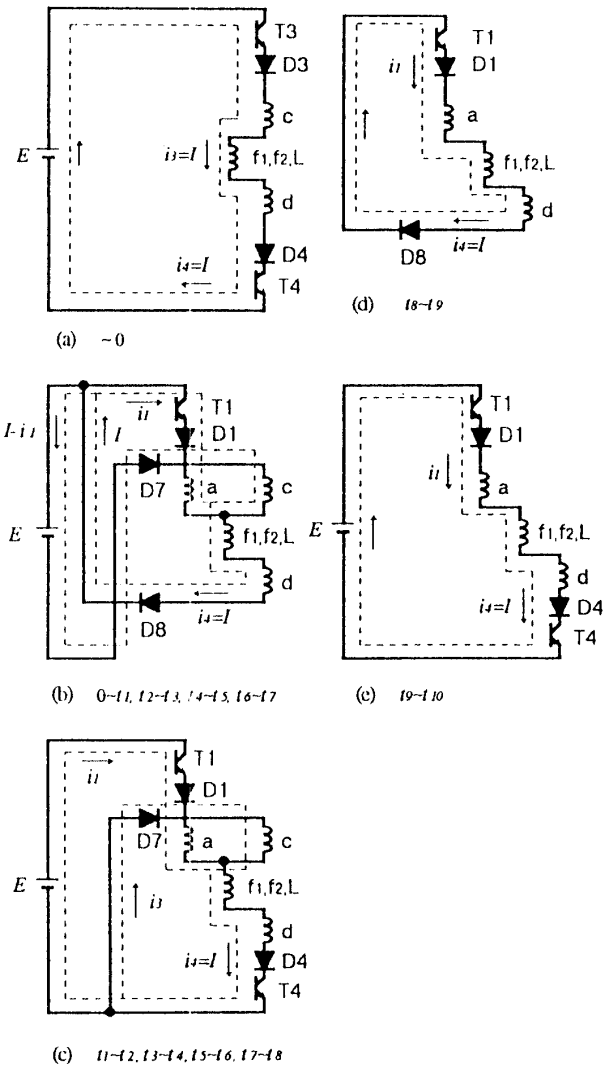

Fig. 4(B) Circuit operations ($u \leq 90°$)

$0 \sim t_1$: the commutation pulse shifts from phase d to phase a, and the armature current commutates from the phase c to the phase a winding in this interval. The phase d is off-state of chopper signal. Feedback power flows from the motor to DC source in this interval, and this value is presented by $E(I-i_1)$.

$t_1 \sim t_2$: phase d is on-state of chopper signal. Active power flows into the motor, and this value is presented by Ei_1.

$t_2 \sim t_3$, $t_4 \sim t_5$, $t_6 \sim t_7$: in these intervals, the circuit operations are identical in interval $0 \sim t_1$.

$t_3 \sim t_4$, $t_5 \sim t_6$, $t_7 \sim t_8$: in these intervals, the circuit operations are identical in interval $t_1 \sim t_2$.

$t_8 \sim t_9$: the commutation of armature current from phase c to phase a winding finishes. The commutation pulse is applied to phase a and chopper signal of phase d are off-state. The power delivery between the motor and DC source does not exist in this interval. This is freewheeling mode.

$t_9 \sim t_{10}$: phase d is on-state of chopper signal. Active power flows into the motor, and this value is presented by EI.

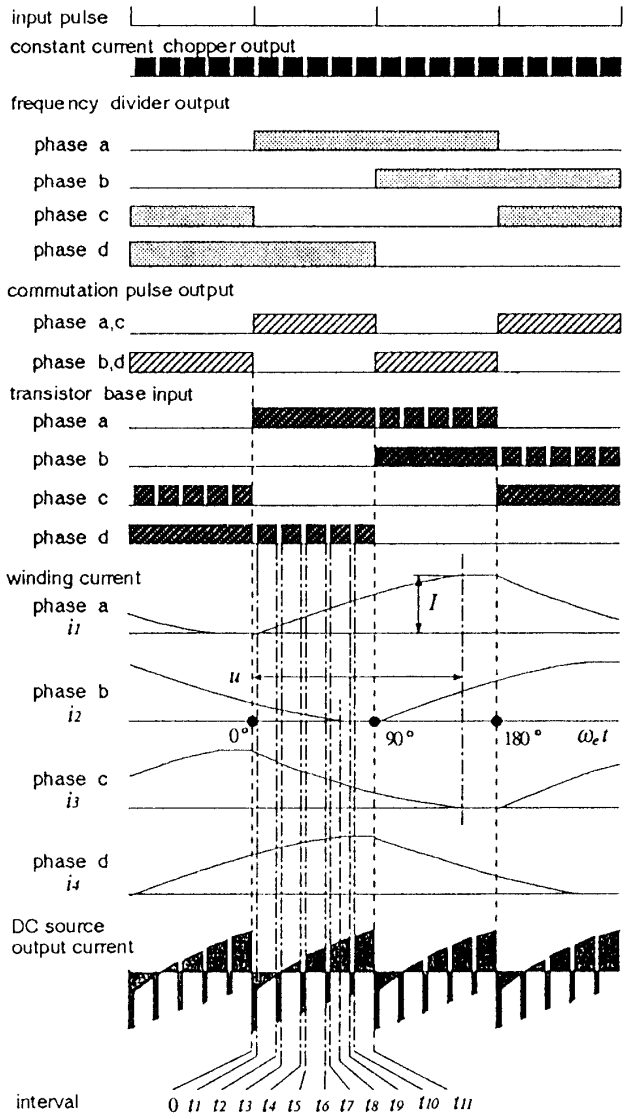

Fig. 5(A) Control signal and current waveforms ($90° \leq u \leq 180°$)

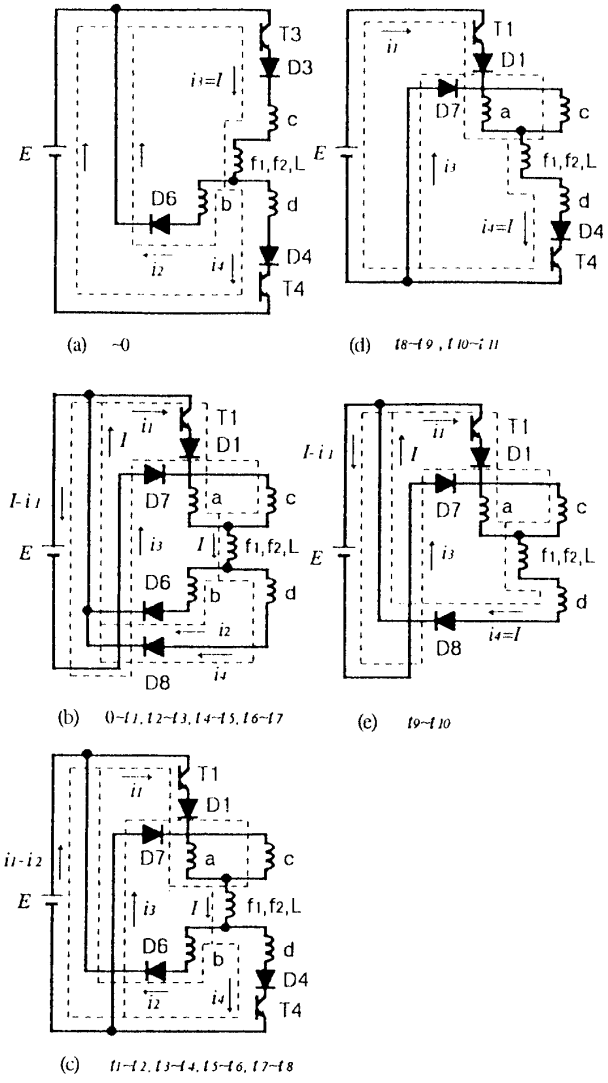

Fig. 5(B) Circuit operations ($90° \leq u \leq 180°$)

(2) $90° \leq u \leq 180°$ (refer to Fig. 5 (A) and Fig. 5 (B))

~0: phase c is on-state of chopper signal, and the commutation pulse is applied to phase d. The feedback current of phase b is still flowing. The case is different from Fig. 4 (A), i.e. Current i_2 flows through freewheeling diode D6. The power flows into the motor in this interval.

$0 \sim t_1$: the commutation pulse shifts from phase d to phase a, and the armature current commutates from phase c to phase a winding in this interval. Phase d is off-state of chopper signal. Feedback power flows from the motor to DC source in this interval, and this value is presented by $E(I-i_1)$. Current i_2 is still flowing.

$t_1 \sim t_2$: phase d is on-state of chopper signal. The bidirectional power flow appears in the interval. This is different from the case of $u \leq 90°$. This input power from DC source to the motor is presented by $E(i_1-i_2)$, and this makes feedback power in negative value. Current i_2 is still flowing.

$t_2 \sim t_3$, $t_4 \sim t_5$, $t_6 \sim t_7$: in these intervals, the circuit operations are identical in interval $0 \sim t_1$.

$t_3 \sim t_4$, $t_5 \sim t_6$, $t_7 \sim t_8$: in these intervals, the circuit operations are identical in interval $t_1 \sim t_2$.

$t_8 \sim t_9$: the commutation of armature current from phase b to phase d finishes. The commutation pulse is applied to phase a and chopper signal of phase d are on-state in this interval. The input power from DC source is Ei_1. This is the same circuit operation as the interval $t_1 \sim t_2$ in Fig. 4 (B).
$t_9 \sim t_{10}$: the chopper signal of phase d is off-state in this interval. Feedback power is $E(I-i_1)$. This is the same circuit operation as the interval $0 \sim t_1$ in Fig. 4 (B).
$t_{10} \sim t_{11}$: the circuit operation is identical in interval $t_8 \sim t_9$.

4. Voltage-current equation and steady state characteristics

The rate of rise of winding current is related to chopper on ratio k as is evident from the current waveforms shown in the preceding chapter. The winding current waveform and pull-out torque characteristics are calculated in consideration of k in the same way as the reference [2] showed.

4.1 Voltage-current equations

On condition that the voltage drop in the armature winding resistance is negligibly small and the fundamental component of armature current is considered, the voltage equation of the system in the heteropolar type shown in Table 1 may be written as follows (See Appendices 8.2):

$$\begin{bmatrix} e_1 \\ e_2 \\ e_3 \\ e_4 \\ e_f \end{bmatrix} = L_c \left\{ \frac{a_2^2}{4} \begin{bmatrix} 3 & 1 & -1 & 1 & 4h \\ 1 & 3 & 1 & -1 & 4h \\ -1 & 1 & 3 & 1 & 4h \\ 1 & -1 & 1 & 3 & 4h \\ 4h & 4h & 4h & 4h & 16h^2 \end{bmatrix} \frac{d}{dt} \begin{bmatrix} i_1 \\ i_2 \\ i_3 \\ i_4 \\ i_f \end{bmatrix} \right.$$

$$+\frac{a_2^2}{4} K\Re \left\{ \begin{bmatrix} 2\gamma^0 & \gamma^0+\gamma^3 & 0 & \gamma^0+\gamma^1 & 4\gamma^0 h \\ \gamma^3+\gamma^0 & 2\gamma^3 & \gamma^3+\gamma^2 & 0 & 4\gamma^3 h \\ 0 & \gamma^2+\gamma^3 & 2\gamma^2 & \gamma^2+\gamma^1 & 4\gamma^2 h \\ \gamma^1+\gamma^0 & 0 & \gamma^1+\gamma^2 & 2\gamma^1 & 4\gamma^1 h \\ 4\gamma^0 h & 4\gamma^3 h & 4\gamma^2 h & 4\gamma^1 h & 0 \end{bmatrix} e^{j\theta_e} \right\} \frac{d}{dt} \begin{bmatrix} i_1 \\ i_2 \\ i_3 \\ i_4 \\ i_f \end{bmatrix}$$

$$\left. +\frac{a_2^2}{4} \omega_e K\Re \left\{ \begin{bmatrix} 2\gamma^1 & \gamma^1+\gamma^0 & 0 & \gamma^1+\gamma^2 & 4\gamma^1 h \\ \gamma^0+\gamma^1 & 2\gamma^0 & \gamma^0+\gamma^3 & 0 & 4\gamma^0 h \\ 0 & \gamma^3+\gamma^0 & 2\gamma^3 & \gamma^3+\gamma^2 & 4\gamma^3 h \\ \gamma^2+\gamma^1 & 0 & \gamma^2+\gamma^3 & 2\gamma^2 & 4\gamma^2 h \\ 4\gamma^1 h & 4\gamma^0 h & 4\gamma^3 h & 4\gamma^2 h & 0 \end{bmatrix} e^{j\theta_e} \right\} \begin{bmatrix} i_1 \\ i_2 \\ i_3 \\ i_4 \\ i_f \end{bmatrix} \right\} \quad (3)$$

where K^2 in the matrix is negligibly small and it disappears from eqn. (3).

The current i_1 and voltage e_1 are obtained from eqn. (3) on condition of

$e_1-e_3=E$ $(0°\leq\omega_e t\leq 90°)$ and $e_1-e_3=kE$ $(90°\leq\omega_e t\leq 180°)$.

These equations are as follows.

$0°\leq\omega_e t\leq 90°$:

$$i_1=0.5E_t/a_2^2 L_c+(a_2+2f_2)KI\{\cos(\omega_e t-\gamma_0)-\cos\gamma_0\}/2a_2 \tag{4}$$

$90°\leq\omega_e t\leq 180°$:

$$i_1=0.5kEt/a_2^2 L_c+0.5(1-k)\pi E/2a_2^2 L_c\,\omega_e + (a_2+2f_2)KI\{\cos(\omega_e t-\gamma_0)-\cos\gamma_0\}/2a_2 \tag{5}$$

$$e_1=a_2^2 L_c[di_1/dt-0.5K(C_1+\omega_e C_2) + K\omega_e I\{(0.25+f_2/a_2)\sin(\omega_e t-\gamma_0)+0.25\cos(\omega_e t-\gamma_0)\}] \tag{6}$$

where

$$C_1=(di_1/dt)\cos(\omega_e t-\gamma_0)+(di_2/dt)\sin(\omega_e t-\gamma_0)$$

$$C_2=-i_1\sin(\omega_e t-\gamma_0)+i_2\cos(\omega_e t-\gamma_0)$$

$\gamma_0=$ a leading angle of fundamental component of winding current for induced voltage.
where

$a_2^2 L_c=L_0$: commutation inductance.
$(a_2^2+2a_2 f_2)KL_c/2=M$: the mutual inductance between armature and DC excitation winding.
$MI\omega_e/0.5E=\Omega$: the ratio of induced voltage to half DC source voltage.

Equation e_1 which is complicated formula may be rewritten with e_1-e_3, since the mean value per period of $i_1\times(e_1-e_3)$ equals to average power per period flowing into the pair of windings (for instance, phase a and c), therefore
$0°\leq\omega_e t\leq 90°$:

$$i_1=MI\omega_e t/L_0\,\Omega+MI\{\cos(\omega_e t-\gamma_0)-\cos\gamma_0\}/L_0 \tag{7}$$

$90°\leq\omega_e t\leq 180°$:

$$i_1=kMI\omega_e t/L_0\,\Omega+(1-k)\pi MI/2L_0\,\Omega+MI\{\cos(\omega_e t-\gamma_0)-\cos\gamma_0\}/L_0 \tag{8}$$

$$e_1-e_3=2\{L_0(di_1/dt)+0.5E\Omega\sin(\omega_e t-\gamma_0)\} \tag{9}$$

The relation between commutating overlap angle u and leading angle γ_0 is obtained for replacing

by $i_1=I$ and $\omega_e t=u$ from eqn. (7) and (8), therefore
$0°\leq\omega_e t\leq 90°$:

$$1-Mu/L_0\,\Omega=M\{\cos(u-\gamma_0)-\cos\gamma_0\}/L_0 \tag{10}$$

$90°\leq\omega_e t\leq 180°$:

$$1-Mu\{k+(1-k)\pi/2u\}/L_0\,\Omega=M\{\cos(u-\gamma_0)-\cos\gamma_0\}/L_0 \tag{11}$$

4.2 Steady state characteristics

In the same way as reference [2], normalized pull-out torque τ_p is given by

$$\begin{aligned}\tau_p=&\cos(u-\gamma_0)+M[\cos\gamma_0+(1-\pi/2)\sin\gamma_0\\&+k\{\sin(u-\gamma_0)-u\cos(u-\gamma_0)-\cos\gamma_0+(\pi/2)\sin\gamma_0\}]/L_0\,\Omega\\&+M[\cos(u-\gamma_0)\{\cos\gamma_0-0.5\cos(u-\gamma_0)\}-0.25(\cos2\gamma_0+1)]/L_0\end{aligned} \tag{12}$$

normalized feedback energy W_f is given by

$$\begin{aligned}W_f=&2M\{\pi/2+k(u-\pi/2)\}/L_0\,\Omega\\&-M^2[k(u-\pi/2)\{k(u-\pi/2)+\pi\}+\pi^2/4]/L_0^2\,\Omega^2\\&-2M^2[\{(1-\pi/2)(1-k)-ku\}\cos\gamma_0+\sin\gamma_0+k\sin(u-\gamma_0)]/L_0^2\,\Omega\end{aligned} \tag{13}$$

As τ_p and W_f mentioned above contain unknown chopper on ratio k, to calculate directly these values is impossible. The k is obtained on condition that the power flowing into the motor equals to the motor effective power. When the pulse speed α [pps] is introduced, the motor input power P_{in} is represented by

$$\begin{aligned}P_{in}=(\alpha E/\omega_e)[&\int_0^{u-\pi/2}[k\{i_1(\theta)-(I-i_1(\pi/2+\theta))\}-(1-k)(I-i_1(\theta))]d\theta\\&+\int_{u-\pi/2}^{\pi/2}\{ki_1(\theta)-(1-k)(I-i_1(\theta))\}d\theta]\end{aligned}$$

by substituting eqn. (4) in the above $i_1(\theta)$ and eqn. (5) in the above $i_1(\pi/2+\theta)$

$$\begin{aligned}P_{in}=(\alpha E/\omega_e)[&MI\{k(u-\pi/2)(k(u-\pi/2)+\pi)+\pi^2/4\}/2L_0\,\Omega\\&+I\{k(\pi-u)-\pi/2\}+MI[\{(1-\pi/2)(1-k)-ku\}\cos\gamma_0\\&+\sin\gamma_0+k\sin(u-\gamma_0)]/L_0]\end{aligned} \tag{14}$$

Equation (14) equals to the motor effective power presented by $4MI^2\omega_e W_m/\pi$ if losses are

neglected; therefore the following equation can be obtained.

$$\Omega W_m = M\{k(u-\pi/2)(k(u-\pi/2)+\pi)+\pi^2/4\}/2L_0\,\Omega + k(\pi-u)-\pi/2+M[\{(1-\pi/2)(1-k)-ku\}\cos\gamma_0 + \sin\gamma_0+k\sin(u-\gamma_0)]/L_0 \quad (15)$$

Where W_m is normalized mechanical output energy in the half cycle. Choosing the appropriate k for some value of Ω in the numerical calculation, some couples of γ_0 and u which are satisfied of conditioned eqns. (10) or (11) exist. A couple of γ_0 and u which has the maximum τ_p (at full-load) and zero τ_p (at no-load) can be found among them. If the obtained γ_0 and u cannot be satisfied of eqn. (15), the preceding procedure is repeated with another k. Finally we determine the most suitable γ_0, u and k which are satisfied of eqns. (10) or (11) and (15), and they make τ_p maximum or zero.

The calculation results of γ_0, u and k for Ω are shown in Figs. 6~8. The machine parameter M/L_0 with a great value means that the field winding has a large number of turns in comparison with the armature winding. The value Ω becomes large in proportion as the motor speed increases. In the case where $\Omega=0.5$ whown in Fig. 6, for instance, leading angle γ_0 enlarges according as the value of parameter M/L_0 decreases. The commutation overlap angle u shown in Fig. 7 represents a similar performance as the γ_0 does. The value of chopper on ratio k, shown in Fig.8, must be increased when the parameter M/L_0 for constant Ω is small.

Fig. 9 shows the calculation result of normalized pull-out torque τ_p for Ω. The value τ_p decreases to the extent of $u=90°\sim180°$ when the parameter M/L_0 for constant Ω is small ($M/L_0=0.18$). Fig. 10 shows the calculation result of normalized feed-back energy W_f for Ω. The value W_f decreases according as the value Ω becomes large in each parameter M/L_0 and the performance is similar to that of τ_p. Fig. 11 shows the calculation result of power ratio ξ of the motor output power to driver capacity for Ω. The value ξ is nearly constant to varied Ω in each parameter M/L_0.

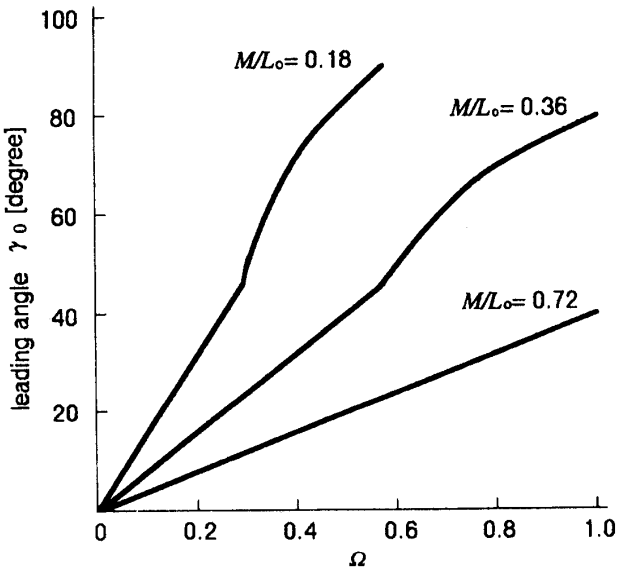

Fig. 6 Leading angle γ_0 vs. Ω characteristics (at full load)

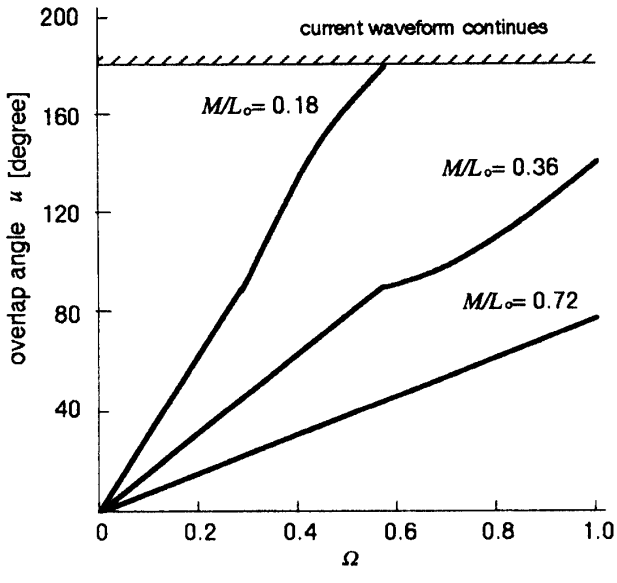

Fig. 7 Commutation overlap angle u vs. Ω characteristics (at full load)

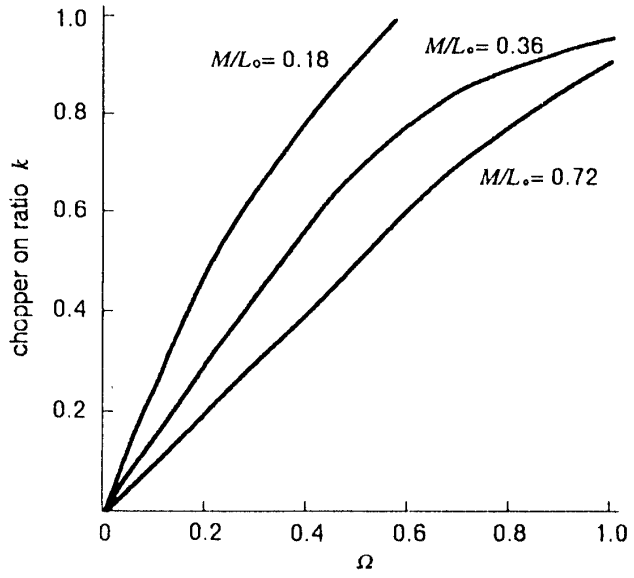

Fig. 8 Chopper on ratio k vs. Ω characteristics (at full load)

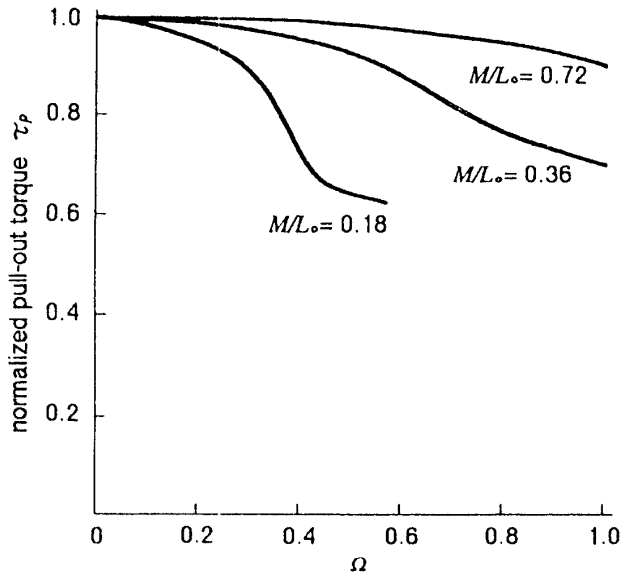

Fig. 9 Normalized pull-out torque τ_p vs. Ω characteristics

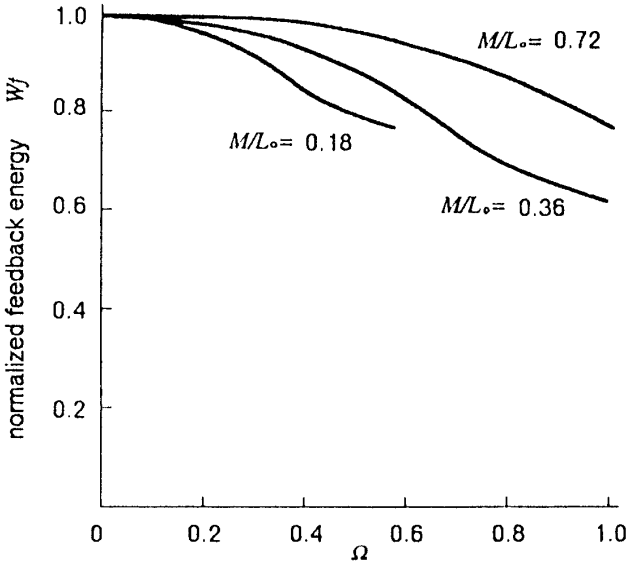

Fig. 10 Normalized feedback energy W_f vs. Ω characteristics

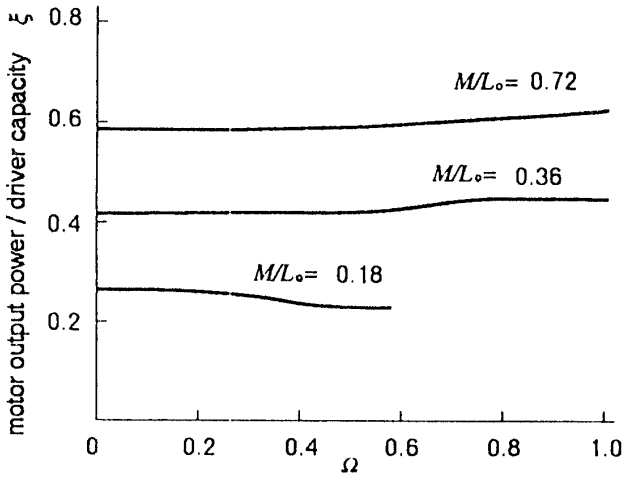

Fig. 11 Motor output power/driver capacity ξ vs. Ω characteristics

5. Comparisons of the calculated and experimental results

5.1 Voltage and current waveforms in winding

When the pulse motor with the constants $\lambda_c=3.22\times10^{-6}$ and $K=0.36$ is driven by this drive circuit, the calculated waveforms of winding voltage (e_2-e_4) and winding current i_2 are shown in Fig. 12, and the measured waveforms in Fig. 13. Comparing Figs. 12 and 13 at no-load operation, the rate of rise of the current i_2 in the measured waveform is larger than that of the calculated waveform. It seems that the matter is due to the influence of iron loss in the motor. In the measured waveforms,

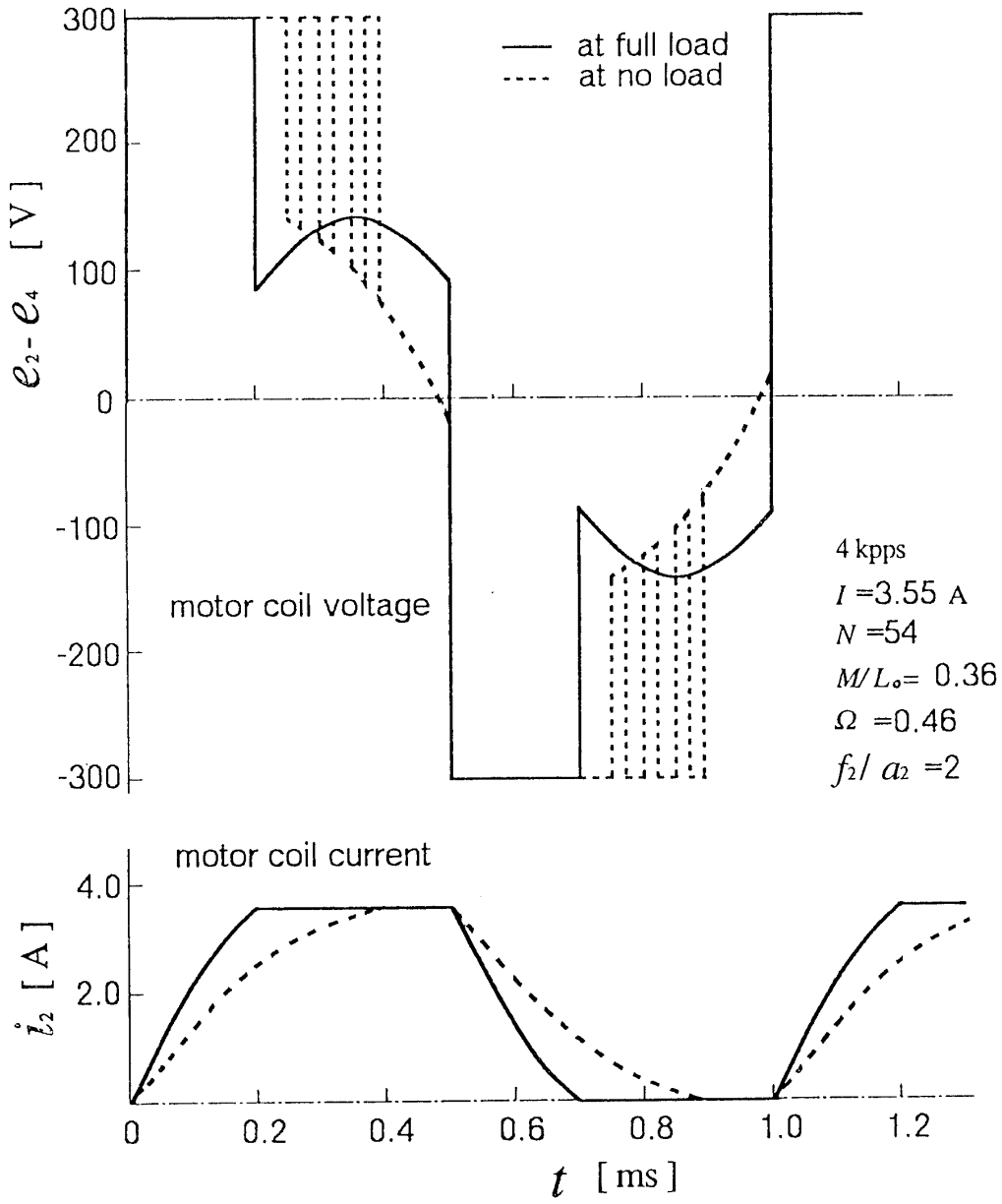

Fig. 12 Calculated waveforms of motor coil voltage and its current

the surge voltage is superposed in the induced voltage waveform at full-load (refer to Fig. 13 (b)). This is caused by the chopper operations. For instance, (refer to Figs. 3 and 4 (A)), immediately after off-state of transistor T2, cathode of the freewheeling diode D6 is clamped by DC source voltage, and the negative surge voltage breaks out in the winding voltage (e_2-e_4). Immediately after on-state of transistor T2, on the other hand, DC source voltage is applied to the winding voltage (e_2-e_4) through the freewheeling diode D8. This is the positive surge voltage.

5.2 Pull-out torque characteristics

Figure 14 shows the calculated and measured pull-out torque characteristics. Pulse speed 4 (10^3 pps) corresponds to the value Ω with 0.46. The pull-out torque in the region of high pulse

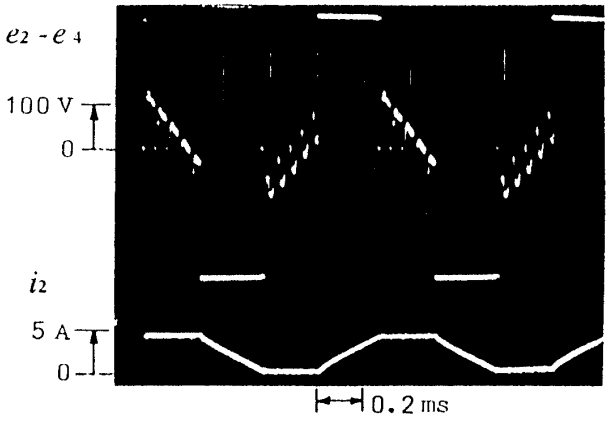

(a) at no load

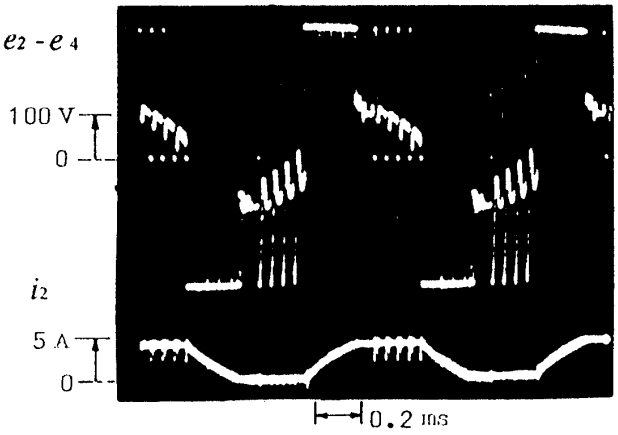

(b) at full load

Fig. 13 Measured waveforms of motor coil voltage and its current

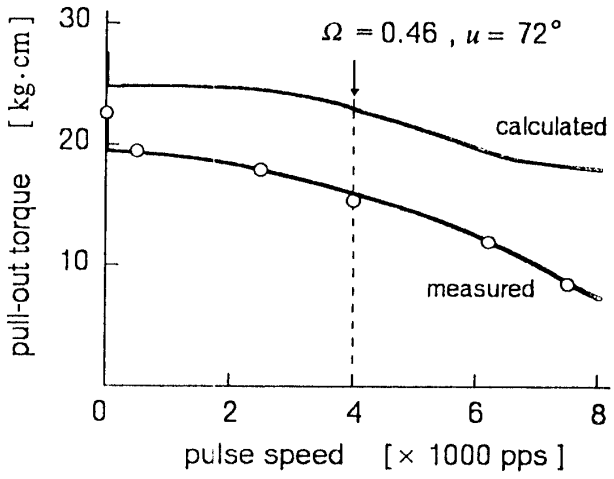

N=54, I=3.55 A , f_2/a_2 =2 , M/L_o= 0.36

Fig. 14 Pull-out torque characteristics

speed falls because the input power is restricted as the chopper on ratio approaches to 1. The performances in the calculation and measurement shown in figure differ because of the losses.

6. Conclusion

The winding method and drive circuit system for the pulse motor have been investigated in the paper. As appropriated for the large capacity system, the number of armature coils was reduced comparing with the conventional form because of reducing the copper loss. The windings were connected in series pairs with the current controlled PWM inverter. The main circuit of this drive system which has four transistors is simplified as compared with the conventional circuit having another chopper circuit. The calculations and experiments were performed in order to obtatin the steady state characteristics. The performances vary in the boundary of commutation overlap angle u=90° in this system. As a result of the investigations, it has been confirmed that the system is usefull for a large capacity pulse motor.

7. References

[1] N. Nagasaka and K. Shinohara, "A study of large-capacity electric pulse motors," *Electrical Engineering in Japan*, vol. 94, no.3, pp.101-109, 1974.

[2] N. Nagasaka and K. Shinohara, "A study of making power up of pulse motor drive system using current type inverter," *Trans. IEE, Japan*, B, vol.95, no.3, pp.9-16, 1975.

[3] J. Benezech, "Le moteur electrique et ses generateurs," *Ingenieurs de Lautomobile*, vol.5, pp.281-301, 1971.

[4] R. Aggarwal and P.P. Acarnley, "Computer-aided selection of variable-reluctance stepping motors," *IEE Proc. B, Electr. Power Appl.*, vol.137, no.4, pp.223-230, 1990.

[5] P.P. Acarnley and A. Hughes, "Machine/drive circuit interactions in small variable-reluctance stepping and brushless DC motor systems," *IEEE Trans. Ind. Electron.*, vol.35, no.1, pp.67-74, 1988

[6] A.P. Russell and I.E.D. Pickup, "An alternative energisation mode for the 4-phase variable-reluctance stepping motor," *IEE Proc. B, Electr. Power Appl.*, vol.129, no.6, pp.355-358, 1982.

[7] D.W.J. Pulle and A. Hughes, "Normalised high-speed performance analysis of small hybrid stepping motors," *IEE Proc. B, Electr. Power Appl.*, vol.134, no.6, pp.333-338, 1987.

[8] A.P. Russell and I.E.D. Pickup, "Calculation of pull-out torque characteristics of hybrid stepping motors with current-regulating drive circuits," *IEE Proc. B, Electr. Power Appl.*, vol.133, no.6, pp.341-346, 1986.

[9] A.P. Russell and I.E.D. Pickup, "A circuital method for the prediction of pull-out torque characteristics of hybrid stepping motors," *IEE Proc. B, Electr. Power Appl.*, vol.129, no.6, pp.330-336, 1982.

8. Appendices

8.1 Calculation of copper loss

Fig. 15 shows the field and armature windings per pole. N is the same total turns in the two forms (the conventionsl form considers one armature winding), and the number of turns of each winding is $f_1 N$, $f_2 N$, $a_1 N$ and $a_2 N$. The field and armature windings have a same conductor size. Fig. 16 shows the connection of windings and duration pattern. Assuming that the average resistance of one turn in the two forms, respectively, is r_1 and r_2, the copper losses Pc_1 and Pc_2 are respectively

$$Pc_1 = I^2 r_1 f_1 N + (1/2) I^2 r_1 a_1 N \times 2$$

$$Pc_2 = I^2 r_2 f_2 N + (1/2) I^2 r_2 a_2 N \tag{16}$$

The following relation holds because of the same two windows.

$$s_1 (f_1 N + 2a_1 N) = s_2 (f_2 N + a_2 N) \tag{17}$$

Where s_1 and s_2 are the sectional areas of a conductor. If the average length of one turn is l, $r_1 = \rho l / s_1$ and $r_2 = \rho l / s_2$ (ρ is a resistivity). From (16) and (17), we have

$$\frac{Pc_2}{Pc_1} = \frac{f_2 + a_2}{f_1 + 2a_1} \cdot \frac{f_2 + a_2/2}{f_1 + a_1} \tag{18}$$

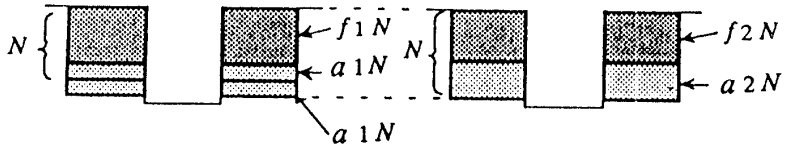

(1) conventional form (2) new form

Fig. 15 Field and armature windings per pole

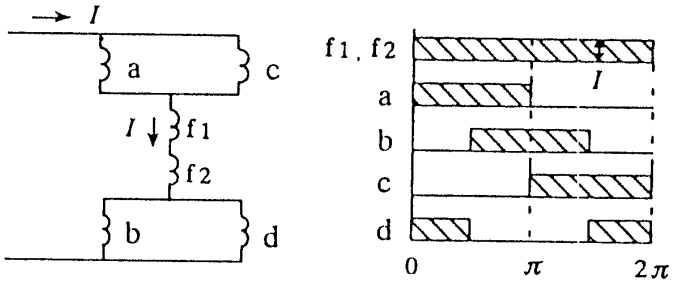

Fig. 16 Connection of windings and duration pattern

Using eqn. (1), the following relation is obtained.

$$\frac{Pc_2}{Pc_1}=\frac{1}{1+2a_1/f_1} \tag{19}$$

For instance, when $f_1/a_1=4$ and $f_2/a_2=1.5$, $Pc_2/Pc_1=0.666$.

8.2 Derivation of eqn. (3)

Fig. 17 shows the basic model of pulse motor which has single salient pole. Assuming that the air-gap permeance distributes sinusoidally in the peripheral direction, the ith permeance λ_i is

$$\lambda_i=\lambda c(1+K\Re[e^{j\theta}\gamma^{i*}]) \tag{20}$$

where $\gamma^i=e^{j2\pi i/n}$, $i=0, 1, 2,\ldots (n-1)$ and sign * denotes conjugate.
The mmf A of the ith exciting coil produces rotor equivalent mmf U as given by

$$(A-U)\lambda_i=U(\Lambda s-\lambda_i) \tag{21}$$

where $\Lambda s=\sum_{k=0}^{n-1}\lambda_k$, and $U=A\lambda_i/\Lambda s$. Magnetic flux interlinkage ϕ_{ik} induced in the kth coil is given by

$$\phi_{ik}=-U\lambda_k=-A\lambda_i\lambda_k/\Lambda s \tag{22}$$

and in the ith coil

$$\phi_{ii}=(A-U)\lambda_i=A\lambda_i-A\lambda_i^2/\Lambda s \tag{23}$$

Denoting $\phi_{ik}=\lambda_{ik}$, when A is unity, Eqn. (22) and (23) can be written as

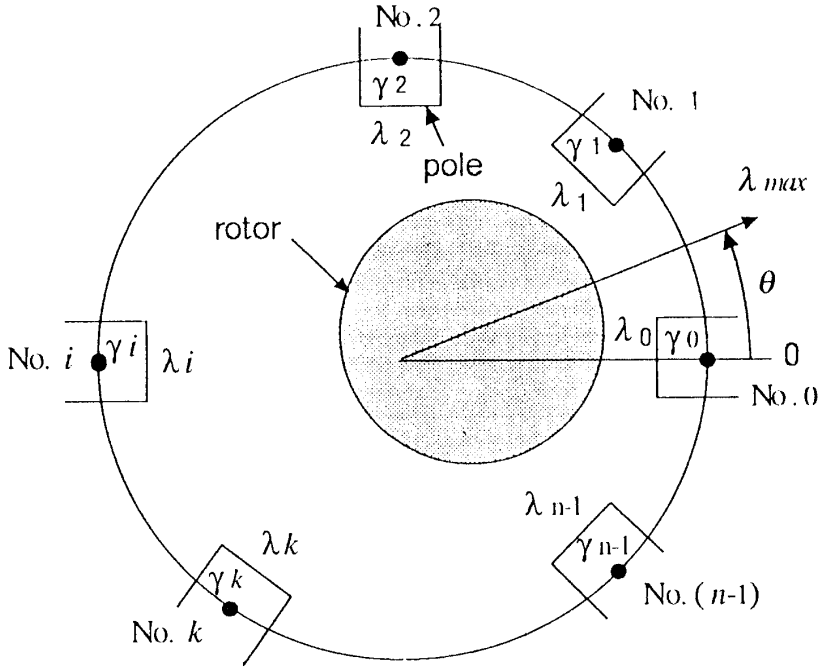

Fig. 17 Basic model of pulse motor

$$\lambda_{ik}=\lambda_i \delta_{ik}-\lambda_i \lambda_k/\Lambda s \tag{24}$$

where $\delta_{ik}=1$ $(i=k)$, $\delta_{ik}=0$ $(i\neq k)$. Substituting Eqn. (20) into (24), λ_{ik} can be expressed as

$$\lambda_{ik}=\lambda c(\delta_{ik}-1/n)+\lambda cK\Re[\gamma^{i*}\delta_{ik}e^{j\theta}]-(\lambda cK/n)\Re[(\gamma^i+\gamma^k)^* e^{j\theta}] \tag{25}$$

where Λs is exchanged to $n\lambda c$ and K^2 is negligible small. When $n=4$, the matrix representation $\boldsymbol{\Lambda}$ of eqn. (25) is as follows.

$$\Lambda=\lambda_c\left[\begin{array}{cccc}1&0&0&0\\0&1&0&0\\0&0&1&0\\0&0&0&1\end{array}-\frac{1}{4}\begin{array}{cccc}1&1&1&1\\1&1&1&1\\1&1&1&1\\1&1&1&1\end{array}\right.$$

$$+K\Re\left\{\left(\begin{array}{cccc}\gamma^0&0&0&0\\0&\gamma^3&0&0\\0&0&\gamma^2&0\\0&0&0&\gamma^1\end{array}\right.\right.$$

$$\left.\left.-\frac{1}{4}\begin{array}{cccc}2\gamma^0&\gamma^0+\gamma^3&0&\gamma^0+\gamma^1\\\gamma^0+\gamma^3&2\gamma^3&\gamma^2+\gamma^3&0\\0&\gamma^2+\gamma^3&2\gamma^2&\gamma^2+\gamma^1\\\gamma^0+\gamma^1&0&\gamma^2+\gamma^1&2\gamma^1\end{array}\right)e^{j\theta}\right\}\Bigg] \tag{26}$$

In general, eqn. (26) is represented as follows.

$$\boldsymbol{\Lambda}_n=\boldsymbol{\Delta}_n-\boldsymbol{M}_n/n \tag{27}$$

where $\boldsymbol{\Delta}_n$ is a diagonal matrix and $\boldsymbol{M}_n$ is a symmetric matrix. The relation between mmf and current ($n=4$) is represented by eqn. (28) which has a transformation matrix $\boldsymbol{C}_n$

$$\begin{array}{|c|}\hline AT_0\\\hline AT_1\\\hline AT_2\\\hline AT_3\\\hline\end{array}=N\begin{array}{|ccccc|}\hline a_2&0&0&0&f_2\\\hline 0&-a_2&0&0&-f_2\\\hline 0&0&a_2&0&f_2\\\hline 0&0&0&-a_2&-f_2\\\hline\end{array}\begin{array}{|c|}\hline i_1\\\hline i_2\\\hline i_3\\\hline i_4\\\hline i_f\\\hline\end{array}$$

$$=N[a_2\boldsymbol{E}_n\quad f_2\boldsymbol{e}_n]\begin{bmatrix}\boldsymbol{i}\\\boldsymbol{i}_f\end{bmatrix}=\boldsymbol{C}_n\begin{bmatrix}\boldsymbol{i}\\\boldsymbol{i}_f\end{bmatrix} \tag{28}$$

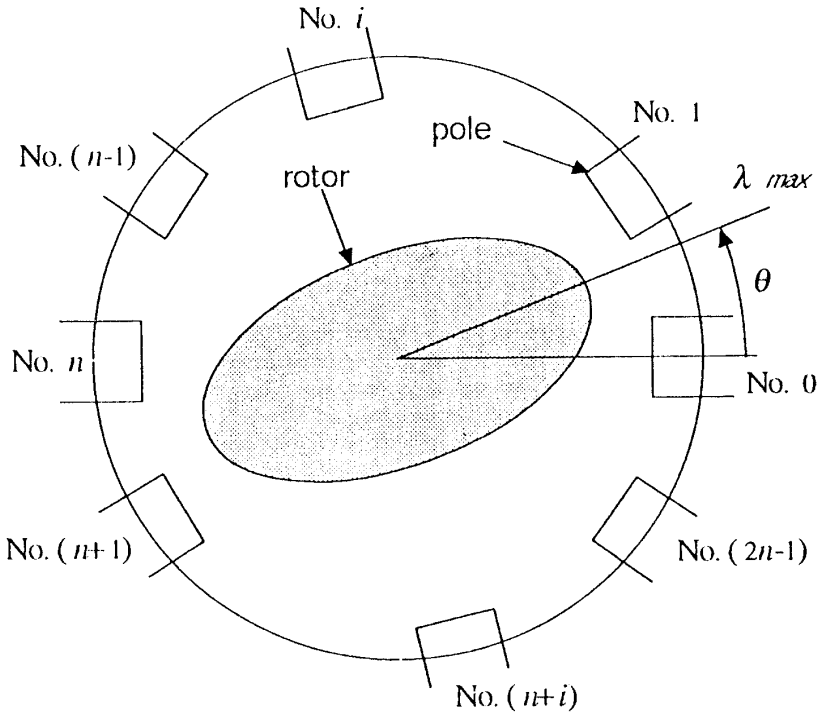

Fig. 18 2-salient poles machine

Fig. 18 shows the practical 2-salient poles machine which has the maximum permeance in the two poles right opposite between the poles. Each time the rotor revolves by 360°, magnetic quantities vary by 720° in electrical angle. Consequently, eqn. (20) to (25) hold without change if γ and θ are replaced by γ^2 and 2θ, respectively. In this case, the permeance matrix $\boldsymbol{\Lambda}_{2n}$ is represented by eqn. (29).

$$\boldsymbol{\Lambda}_{2n}=\begin{bmatrix} \boldsymbol{\Delta}_n-\boldsymbol{M}_n/2n & -\boldsymbol{M}_n/2n \\ -\boldsymbol{M}_n/2n & \boldsymbol{\Delta}_n-\boldsymbol{M}_n/2n \end{bmatrix} \tag{29}$$

The coil matrix $\boldsymbol{C}_{2n}$ is given by

$$\boldsymbol{C}_{2n}=N\begin{bmatrix} a_2\boldsymbol{E}_n & f_2\boldsymbol{e}_n \\ a_2\boldsymbol{E}_n & f_2\boldsymbol{e}_n \end{bmatrix} \tag{30}$$

The inductance matrix $\boldsymbol{L}$ can be obtained using matrix $\boldsymbol{C}_{2n}$ and $\boldsymbol{\Lambda}_{2n}$ as follows.

$$\boldsymbol{L}=\boldsymbol{C}_{2n}{}^{T}\,\boldsymbol{\Lambda}_{2n}\,\boldsymbol{C}_{2n} \tag{31}$$

Calculating eqn. (31) in $2n=8$, the inductance matrix of heteropolar type is obtained as shown in Table 1. Voltage current equation is

$$[e]=\frac{d}{dt}\{[L][i]\}=[L]\frac{d[i]}{dt}+\frac{d[L]}{dt}[i] \tag{32}$$

where $[e]$ and $[i]$ are the voltage and current in each coil as shown in eqn. (3), respectively.